Angewandte Chemie International Edition

Angewandte International Edition Chemie

How to cite: *Angew. Chem. Int. Ed.* **2026**, e5507499
doi.org/10.1002/anie.5507499

RESEARCH ARTICLE

Palladium-Catalyzed Regiodivergent Telomerization of Isoprene With Oxindoles

Ying-Ying Liu[1,2] | Shao-Han Sun[1,2] | Xue-Ting Li[1,2] | Zhi-Hui Wang[1,2] | Ding-Wei Ji[1] | Xiang-Ping Hu[1,2] | Qing-An Chen[1,2]

[1]Dalian Institute of Chemical Physics, Chinese Academy of Sciences, Dalian, People's Republic of China | [2]University of Chinese Academy of Sciences, Beijing, People's Republic of China

Correspondence: Ding-Wei Ji (dingweiji@dicp.ac.cn) | Xiang-Ping Hu (xiangping@dicp.ac.cn) | Qing-An Chen (qachen@dicp.ac.cn)

Received: 9 April 2026 | **Revised:** 24 April 2026 | **Accepted:** 13 May 2026

Keywords: BPMO ligands | DFT analysis | isoprene | telomerization

ABSTRACT

Transition metal-catalyzed nucleophilic telomerization of isoprene is an efficient strategy for the construction of monoterpene skeletons, yet its development has been impeded by inherent challenges of chemo- and regioselectivity control, especially in reactions with carbon nucleophiles. Herein, we developed a versatile palladium catalysis for the regiodivergent telomerization of isoprene with oxindoles through synergistic control of ligands, solvents, and additives. In the presence of aprotic solvent NMP, we revealed the electron-rich and less bulky tri(2-furyl)phosphine (TFP) ligand can facilitate the exclusive formation of tail-to-tail geranyl oxindoles, meanwhile the reactivity was severely improved by adding base as additive. On the other hand, a newly designed hemilabile phosphine ligand enables selective access to tail-to-head isomer, where the MeOH worked as an irreplaceable solvent choice. Mechanistic experiments and density functional theory (DFT) calculations were conducted, which indicate that protolysis of the η^1,η^3-diallyl–Pd(II) complex is speculated to be the rate-determining step. Apart from oxindoles, this regiodivergent protocol could also be applied to the nucleophilic telomerization of isoprene with a broad scope of amines. Furthermore, the synthetic utility of current synthetic strategy was illustrated by late-stage alkene isomerization, as well as various derivatizations that effectively expand the structural diversity of monoterpenoids and complement alkaloid frameworks.

1 | Introduction

Monoterpenoids are a large and diverse group of naturally occurring compounds whose basic structure consists of two isoprene units [1, 2], playing an irreplaceable role in pharmaceuticals or agrochemicals due to their diverse bioactivities [3–5]. Besides, owing to their characteristic odor and taste, many monoterpenoids or their derivatives have also been applied in cosmetic materials [6], food flavors [7], or insect repellents [8, 9]. Although acyclic monoterpenoids can be structurally classified into four types—head-to-tail (*H-T*), tail-to-tail (*T-T*), tail-to-head (*T-H*) and head-to-head (*H-H*) coupling products—based on the different coupling sites of isoprene unit [10, 11], most natural monoterpenoids are found only with *H-T* coupling backbone [12, 13]. This is mainly because the biosynthesis of monoterpenes relies on the transformation of geranyl diphosphate (GPP) intermediate, which is generated through enzymatic condensation of isopentenyl pyrophosphate (IPP) and dimethylallyl pyrophosphate (DMAPP) (Figure 1A) [14–16]. To overcome such limitation and expand the structural diversity of terpenoids beyond, sustained efforts have been devoted to artificial catalysis in past decades to enable the construction of

Ying-Ying Liu and Shao-Han Sun contributed equally to this work.

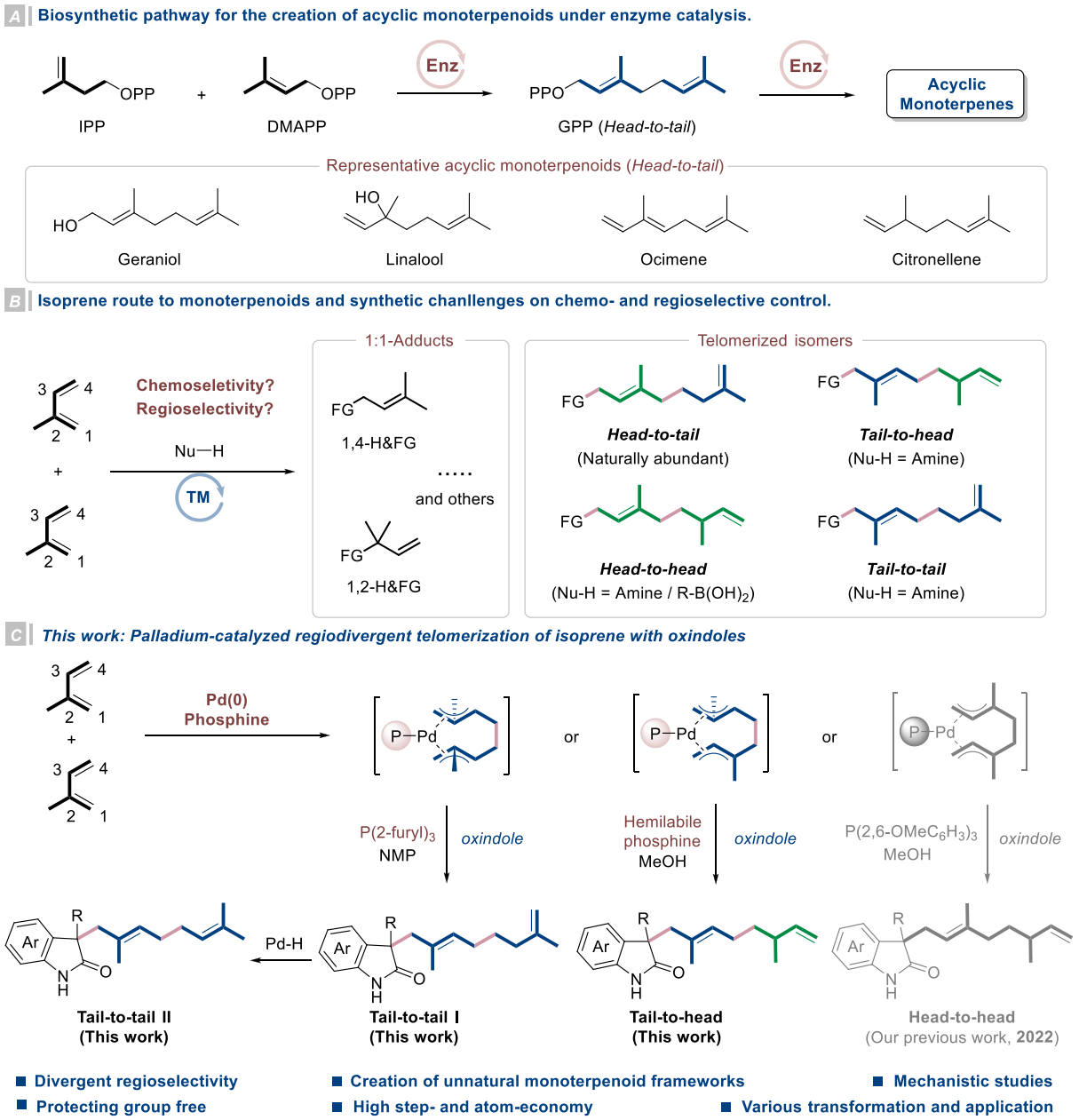

FIGURE 1 | Catalytic constructions of acyclic monoterpenoids.

monoterpenoid skeleton liberating from naturally existing *H-T* selectivity [17–25].

Isoprene is not only an important bulk fossil chemical but also the most abundant hydrocarbon in the atmosphere after methane, emitted via plant biogenic processes. In theory, the catalytic telomerization of renewable isoprene can serve as a transformative step for the construction of monoterpenoid backbones [26–29]. However, isoprene contains an internal methyl group and represents the smallest non-symmetrically substituted 1,3-diene. The telomerization of isoprene has been challenging as it can generate up to four regioisomers (head-to-tail, tail-to-tail, and tail-to-head telomers). In addition, achieving chemoselectivity over direct X–H addition reactions, as well as suppressing its self-dimerization, further complicates the reaction outcomes. In contrast to the success achieved with 1,3-butadiene [30], very few catalytic systems have been developed to enable good selectivity in isoprene telomerization [31–38]. Successful examples reported by Finn, Réau, and Castillon et al. mainly focus on C—N bond construction with diethylamine (Figure 1B) [32, 34, 39]. However, selectivity control using more challenging carbon nucleophiles remains in its infancy.

Oxindoles and their derivatives are prevalent structural motifs in numerous natural products and synthetic pharmaceutical molecules [40, 41]. In 2022, we achieved excellent head-to-head selectivity in the Pd-catalyzed telomerization of isoprene with oxindoles by employing a bulky phosphine ligand [35]. Very recently, this strategy was successfully extended to nickel-catalyzed arylative head-to-head telomerization using boronic acids [38]. Given that monoterpenes with head-to-tail selectivity can be readily accessed via nucleophilic substitution with bio-

TABLE 1 | Reaction optimization for tail-to-tail (*T-T*) telomerization of isoprene with oxindole.

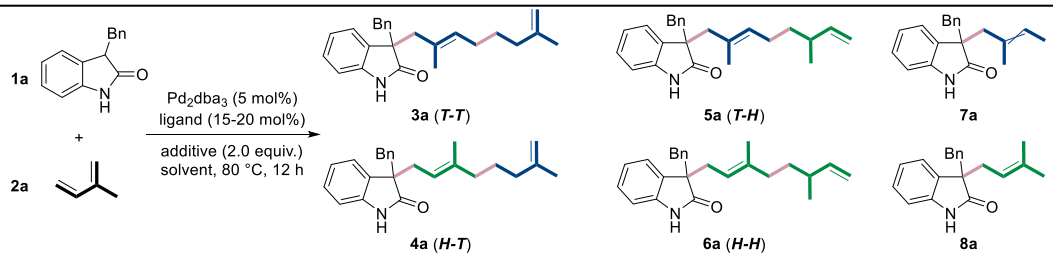

Entry	Ligand (x mol%)	Additive	Solvent	Yield (%)					
				3a	4a	5a	6a	7a	8a
1	PPh_3 (15)	Et_3N	DMF	53	6	2	1	—	—
2	PPh_2Cy (15)	Et_3N	DMF	12	5	—	1	—	—
3	P(4-$MeC_6H_4)_3$(15)	Et_3N	DMF	4	2	—	—	—	—
4	P(4-$ClC_6H_4)_3$(15)	Et_3N	DMF	—	—	—	—	—	—
5	P(3-$MeC_6H_4)_3$(15)	Et_3N	DMF	15	2	3	—	—	—
6	P(2-$MeOC_6H_4)_3$ (15)	Et_3N	DMF	37	21	—	—	—	—
7	Ph-JohnPhos (15)	Et_3N	DMF	17	9	—	—	—	—
8	P(2-furyl)$_3$ (15)	Et_3N	DMF	59	6	—	—	—	—
9	P(2-furyl)$_3$ (20)	Et_3N	DMF	61	8	—	—	—	—
10	P(2-furyl)$_3$ (20)	Et_3N	NMP	69	6	—	—	—	—
11	P(2-furyl)$_3$ (20)	Et_3N	MeOH	31	2	17	21	5	8
12	P(2-furyl)$_3$ (20)	Et_3N	^{i}PrOH	52	11	—	4	2	2
13	P(2-furyl)$_3$ (20)	$^i Pr_3N$	NMP	60	8	—	—	—	—
14	P(2-furyl)$_3$ (20)	DABCO	NMP	84	3	—	—	—	—
15	P(2-furyl)$_3$ (20)	DBU	NMP	45	5	—	—	—	—
16	P(2-furyl)$_3$ (20)	—	NMP	26	—	—	—	—	—

Note: Condition: **1a** (0.10 mmol), **2a** (0.80 mmol), Pd_2dba_3 (5 mol%), ligand (15–20 mol%), additive (2.0 equiv.), solvent (0.2 mL), 80°C, 12 h. Yields were determined by GC-FID analysis of the crude product mixture using mesitylene as internal standard.

Abbreviations: Ph-JohnPhos, 2-(diphenylphosphino)biphenyl; DBU, 1,8-diazabicyclo[5.4.0]undec-7-ene; DABCO, 1,4-diazabicyclo[2.2.2]octane.

derived geraniol, the controlled synthesis of the remaining two telomers (tail-to-tail and tail-to-head) is of great significance for enriching monoterpene structural diversity. In continuation of our long-standing interest in the catalytic transformation of isoprene [36, 37, 42–46], we herein report the development of a ligand-regulated regiodivergent telomerization of isoprene with oxindoles under Pd catalysis. Using the less sterically hindered tri(2-furyl)phosphine (TFP) ligand, geranyl oxindoles with tail-to-tail selectivity were obtained with high chemo- and regioselectivity, while the tail-to-head telomer could be accessed by regulation with a newly designed and synthesized hemilabile phosphine ligand (Figure 1C). This work provides a novel paradigm for the synthesis of skeleton-divergent terpenoids beyond naturally occurring cores (Figures 2–5).

2 | Results and Discussion

Initially, 3-benzyloxindole (**1a**) and isoprene (**2a**) were selected as model substrates under palladium catalysis in *N*,*N*-dimethylformamide (DMF) with Et_3N as additive (Tables 1 and S1–S5). Under the catalysis of $Pd(OAc)_2$ and PPh_3, the telomerization reaction delivered 60% yield of *T-T* coupling isomer (**3a**), as well as 25% yield of tail-to-head product **5a** and 3% yield of C5-product **7a** (Tables S1, entry 1). The assessment of palladium catalyst precursors showed that $Pd(PPh_3)_4$ exhibited higher yield of **3a** than $Pd(OAc)_2/PPh_3$, but Pd_2dba_3 showed better selectivity (Table S1, entries 2–5). Therefore, we chose Pd_2dba_3 for further evaluation of ligands (Tables 1 and S2). The optimization of ligands revealed that phosphine ligands substituted by alkyl group would diminish the reaction yields (Table 1, entry 2 and see Table S2 for details). Among all tested triarylphosphine ligands, P(2-furyl)$_3$ displayed the highest reactivity and regioselectivity, affording **3a** and **4a** in 59% and 6% yields, respectively (Table 1, entries 1–8). And the yield of **3a** can be further increased to 61% yield when 20 mol% of P(2-furyl)$_3$ was loaded (Table 1, entry 9). Then solvents were screened, disclosing that this reaction was generally facilitated by aprotic polar solvents, as a considerable loss of selectivity could be observed when MeOH employed (Table 1, entries 9–12 and Table S3). The *N*-methyl-2-pyrrolidone (NMP) proved to be the best choice, giving product **3a** in 69% yield, accompanied by 6% yield of **4a** (Table 1, entry 10), Apart from Et_3N, other additives including organic or inorganic bases, acids, and water, were also surveyed (Table 1, entries 12–15 and

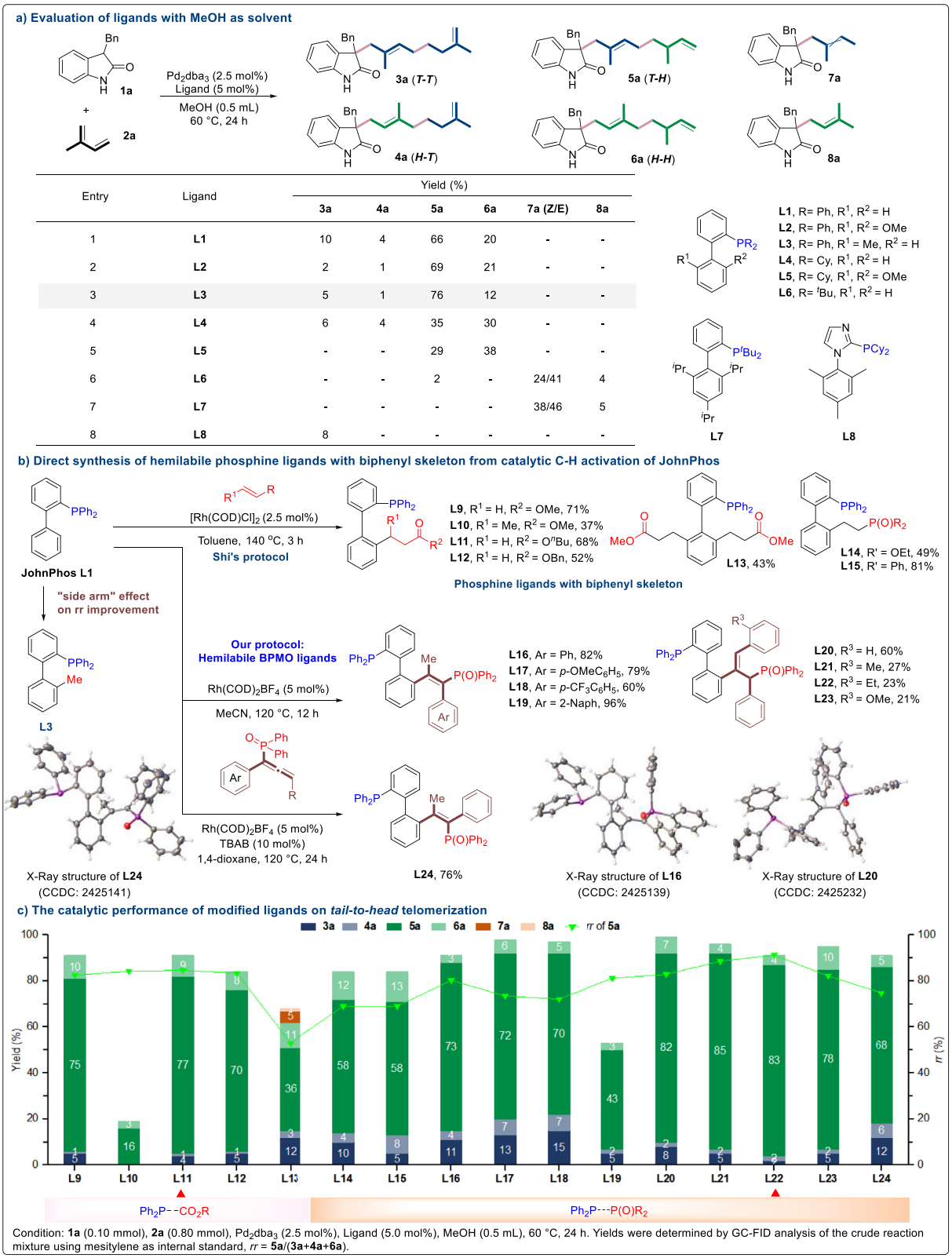

Entry	Ligand	Yield (%)					
		3a	4a	5a	6a	7a (Z/E)	8a
1	L1	10	4	66	20	-	-
2	L2	2	1	69	21	-	-
3	L3	5	1	76	12	-	-
4	L4	6	4	35	30	-	-
5	L5	-	-	29	38	-	-
6	L6	-	-	2	-	24/41	4
7	L7	-	-	-	-	38/46	5
8	L8	8	-	-	-	-	-

Condition: **1a** (0.10 mmol), **2a** (0.80 mmol), Pd_2dba_3 (2.5 mol%), Ligand (5.0 mol%), MeOH (0.5 mL), 60 °C, 24 h. Yields were determined by GC-FID analysis of the crude reaction mixture using mesitylene as internal standard, *rr* = **5a**/(**3a**+**4a**+**6a**).

FIGURE 2 | Reaction optimization for tail-to-head (*T-H*) telomerization of isoprene with oxindole.

Table S4). To our delight, the *T-T* telomer **3a** was produced in 84% yield with excellent regioselectivity by adding DABCO (entry 14). The regioisomer distribution (**3a**: 84% yield, **4a**: 3% yield, **5a**: not detected, **6a**: not detected) was determined as 97:3:0:0, which matched the theoretical calculations excellently (94:5:<1:<1; see detailed discussion for Figure 6 and Page S76). In comparison, the telomerization reaction exhibited a significant loss of reactivity in the absence of additive (Table 1, entry 16).

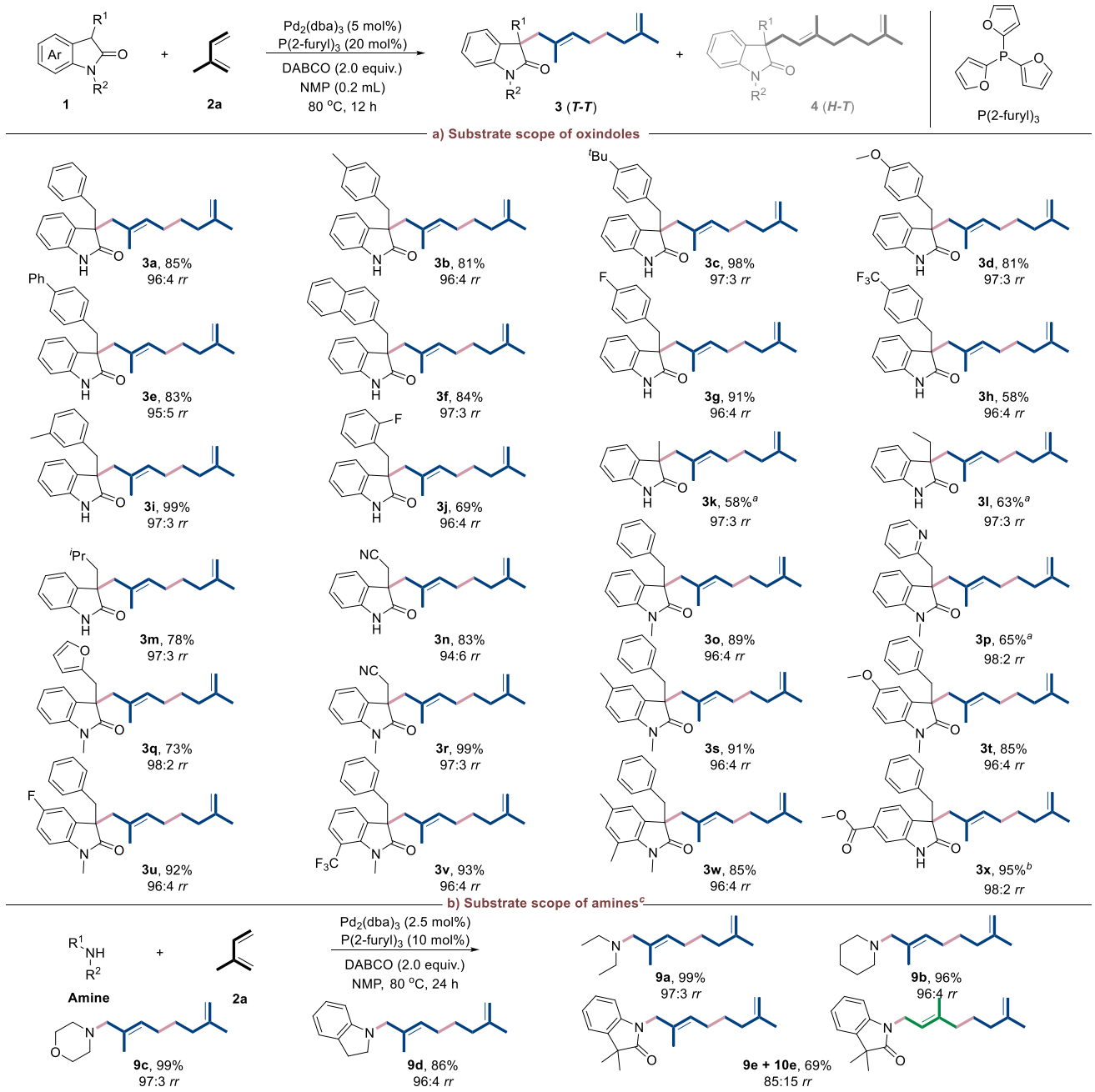

Conditions: **1** (0.10 mmol), **2a** (0.80 mmol), $Pd_2(dba)_3$ (5 mol%), P(2-furyl)$_3$ (20 mol%), DABCO (0.20 mmol), NMP (0.2 mL), 80 °C, 12 h. [a]24 h. [b]8 h. [c] **Amine** (0.20 mmol), **2a** (1.60 mmol), $Pd_2(dba)_3$ (2.5 mol%), P(2-furyl)$_3$ (10 mol%), DABCO (0.40 mmol), NMP (0.2 mL), 80 °C, 24 h. Isolated yields were given in all cases. The *rr* =***TT***/(***HT***+***TH***+***HH***), determined by ^{1}H NMR analysis of isolated products.

FIGURE 3 | Substrate scope of tail-to-tail telomerization of isoprene with oxindoles and amines.

Controlled experiments showed that the reactions catalyzed by $Pd_2(dba)_3$ still performed better than those with $Pd(PPh_3)_4$ and $Pd(OAc)_2$ in NMP (Table S5).

Previously, we have demonstrated that excellent head-to-head selectivity (*H-H*, **6a**) could be achieved under palladium catalysis with bulky phosphine ligand P(2,6-$MeOC_6H_3$)$_3$ when using MeOH as solvent [35]. It was also noted that the tail-to-head product **5a** was also slightly facilitated under current condition in MeOH (Table 1, entry 11). Inspired by these results, further ligand screening was conducted with MeOH as solvent to improve the tail-to-head (**5a**) selectivity (Figure 2a and Table S6). The results showed that triaryl phosphine ligands bearing a biphenyl skeleton moderately switched the selectivity toward the tail-to-head product **5a** (Figure 2a, entries 1–8). When 2-(diphenylphosphino)biphenyl (Ph-JohnPhos, **L1**) was employed, **5a** was detected as the dominant product in 66% yield, along with other isomers (entry 1). Ligands with a substituent at the *ortho*-position of the biphenyl skeleton (**L2** and **L3**) successfully improved the yield of **5a** to 69% and 76%, respectively. Replacing the phenyl groups with cyclohexyl groups (**L4–L5**) impeded current telomerization reactions, likely due to the increased electron density or steric hindrance (entries 4 and 5). This trend became even more pronounced with tert-butyl-substituted

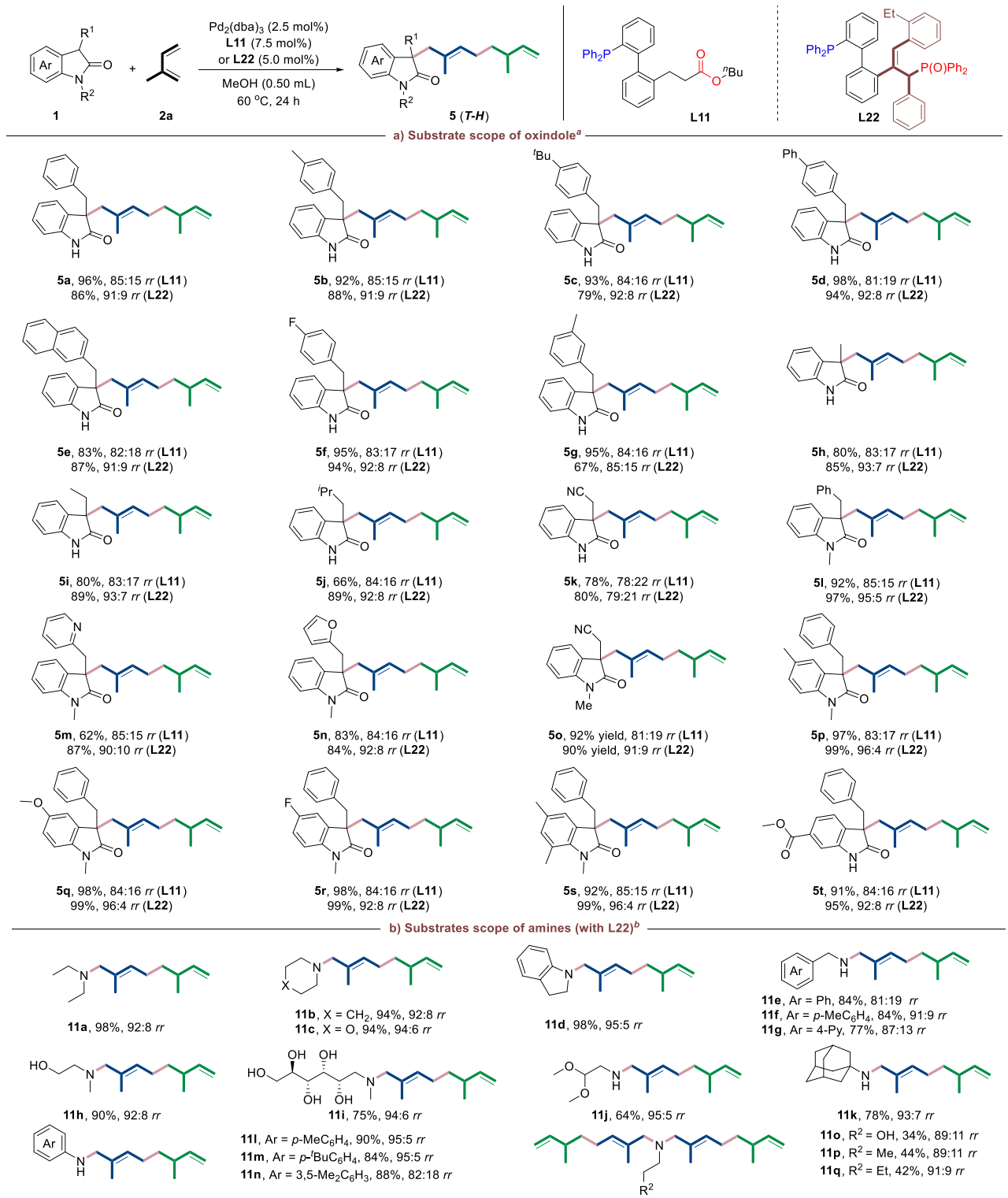

[a]**Conditions**: **1** (0.10 mmol), **2a** (0.80 mmol), $Pd_2(dba)_3$ (2.5 mol%), **L11** (7.5 mol%) or **L22** (5.0 mol%), MeOH (0.5 mL), 60 °C, 24 h. [b]**Amine** (0.50 mmol), **2a** (2.0 mmol), $Pd_2(dba)_3$ (0.5 mol%), **L22** (0.5 mol%), MeOH (0.5 mL), 60 °C, 24 h. Isolated yields were given in all cases. The *rr* = ***TH***/(***TT***+***HT***+***HH***), determined by ^{1}H NMR analysis of isolated products. 1:1 *dr was obtained in all cases.*

FIGURE 4 | Substrate scope of tail-to-head telomerization or isoprene with oxindoles and amines.

phosphine ligands (**L6–L7**), for which the corresponding telomerization reactions were almost completely suppressed (entries 6 and 7). Ligand **L8** showed good reactivity in previous tail-to-head telomerization of isoprene with diethylamine [32], but only afforded 8% yield of **3a** in current reaction (entry 8). Compared with diethylamine, the oxindole is a kind of weaker nucleophile with larger steric hindrance, thus calling for a more delicate decoration on Ph-JohnPhos skeleton. The investigation of other solvent indicated that the success of current tail-to-head telomerization highly depended on MeOH

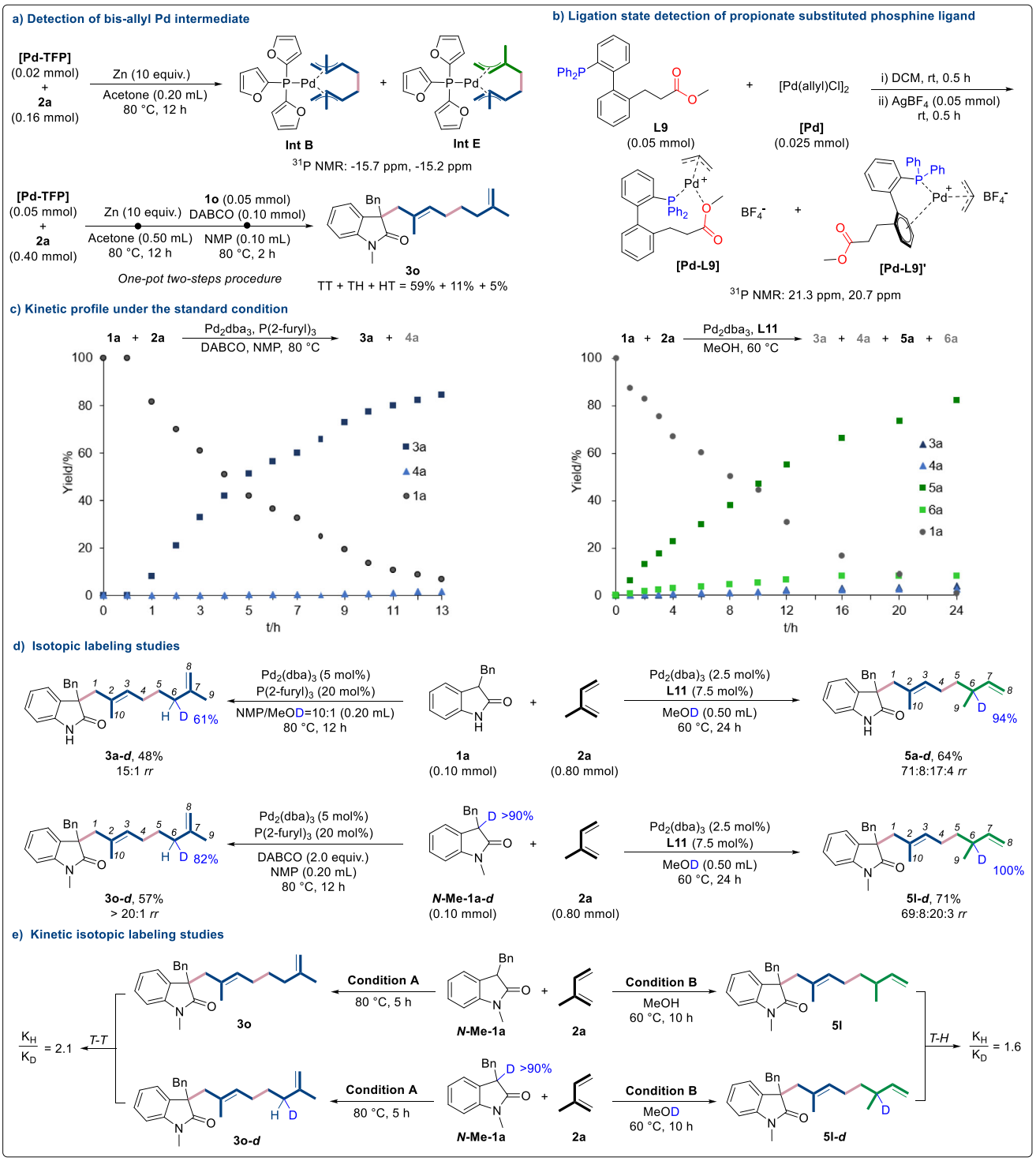

FIGURE 5 | Mechanistic investigations.

(see Table S7). Replacing MeOH with other protic solvents would cause a thorough loss of reactivity, probably by influencing the protolysis process. Precedented work by Castillon et al. has revealed that the alcohol solvents controlled the regioselectivity as a function of its pK_a, leading to a continuous shift of the selectivity-determining step [32]. The examination of commonly used palladium precursors disclosed that Pd_2dba_3 exhibited higher yield and regioselectivity of product **5a** (Table S8).

Motivated by the promising "side arm" effect on selectivity improvement, we set out to optimize the yield and selectivity of **5a** by decorating the *ortho*-position of the Ph-JohnPhos ligand via a P(III)-directed C–H activation strategy (Table S9). Adopting a protocol developed by Shi et al. [47–50], hemilabile phosphine ligands **L9-L15** were synthesized through Rh-catalyzed C–H alkylation of the commercially available ligand **L1** with activated alkenes (Figure 2b). As expected, telomerization reactions with

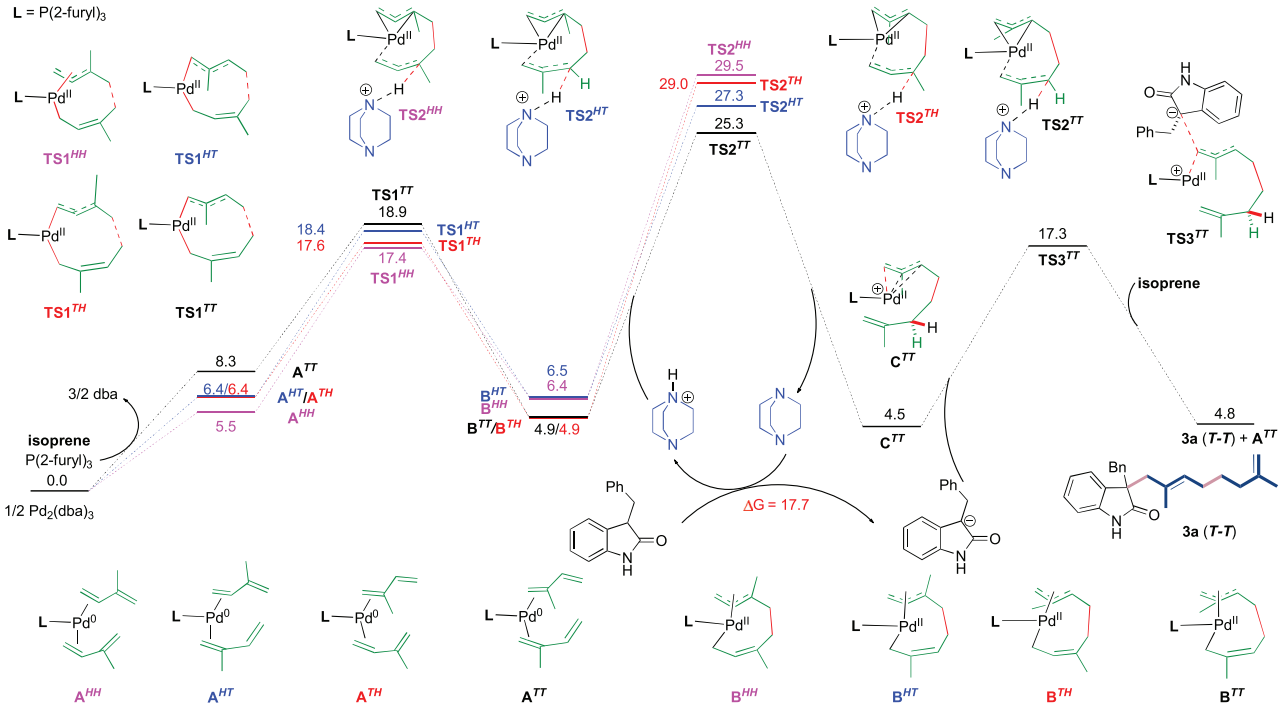

FIGURE 6 | DFT calculations for the tail-to-tail telomerization with $P(2\text{-furyl})_3$ as ligand in NMP. B3LYP-D3BJ/SDD (Pd), 6-311+G(d,p)/SMD(NMP)//B3LYP/lanl2dz (Pd), and 6-31G(d,p) 80°C (353.15 K).

these hemilabile ligands all showed a preference for the T–H coupling product **5a** (Figure 2c, **L9**-**L15**). Comparatively, ligands bearing a propionic ester group (**L9, L11, and L12**) significantly enhanced both reactivity and selectivity. Among them, ligand **L11** with *n*-butyl propionate exhibited best performance, affording the *T-H* product **5a** in 77% yield and 85% *rr*. By increasing the loading of **L11** to 7.5 mol%, the yield of **5a** was further improved to 82%, accompanied by a small portion of regioisomers (**3a**: 4% yield, **4a**: 1% yield, **6a**: 8% yield, see Table S19, entry 4). The product ratio **3a**/**4a**/**5a**/**6a** was calculated to be 4:1:87:8, in good agreement with the theoretical isomer distribution (see detailed discussion for Figure 7 and Page S78). The mixed solvents of different alcohols with MeOH (1:1) were also examined, nevertheless, led to a considerable loss of selectivity (Table S20). Increasing the steric hindrance of the ligands (**L10** and **L13**) proved detrimental to the reaction outcomes. In addition, replacing the ester group with a phosphorus unit—affording bisphosphine monoxide (BPMO)-type hemilabile ligands—also enabled the reaction, albeit with relatively lower efficiency (**L14** and **L15**).

The above promising results inspired us to further modify the ligand skeleton by incorporating an allene unit (Figure S1) [51–53]. After extensive attempts, a modified Rh-catalyzed protocol was successfully developed via P(III)-directed C–H alkenylation with allenyl phosphine oxide (Figure 2a and Tables S10–S15). Using $Rh(COD)_2BF$ as pre-catalyst, BPMO ligands **L16**-**L23** were afforded in 21%–96% yields as either (*E*)-*β,γ*-adducts or (*E*)-*α,β*-adducts, depending on the *γ*-substituent of allenyl phosphites. Remarkably, the stereoselectivity could be inverted by employing a catalytic amount of tetrabutylammonium bromide (TBAB), affording the *Z*-configured *β,γ*-adduct **L24** in good yield. The structures of ligands **L16**, **L20**, and **L24** were further confirmed by single-crystal x-ray crystallography (CCDC 2425139, 2425232, and 2425141) [54]. With these new BPMO ligands in hand, we subsequently evaluated their performance in the *T-H* telomerization of isoprene with oxindole (Figure 2b, **L16-24**). Gratifyingly, although ligands with a tetrasubstituted alkene motif (**L16-18, L24)** exhibited considerable telomerization reactivity and regioselectivity comparable to **L11**, a remarkable improvement in yield and *T-H* selectivity was observed when using the (*E*)-*α,β*-adducts **L20–23** as ligands. Variation of the substituents revealed that the ethyl-substituted BPMO ligand **L22** was optimal in terms of regioselectivity, delivering the *T-H* product **5a** in 83% yield.

With the optimized conditions in hand, the substrate generality of Pd-catalyzed tail-to-tail telomerization was subsequently tested in the presence of $P(2\text{-furyl})_3$ and DABCO (Figure 3a). Subjecting 3-Bn substituted oxindole **1a** to standard conditions furnished geranyl oxindole **3a** in 85% yield and 96:4 *rr*. The benzyl groups, regardless of the electron-donating groups (Me, ^{t}Bu, OMe) or electron-withdrawing groups (F, Ph) at its *para* position, were all well-tolerated to afford corresponding products in 81%–98% yields with regioselectivity maintained at high levels (**3b**-**3e**, **3g**). While 3-(p-CF_3-Bn) or 3-(*o*-F-Bn) substituted oxindoles gave products (**3h**, **3j**) in slightly inferior yields (58%–69%), 3-(2-naphthylmethyl) and 3-(*m*-Me-Bn) substituted oxindoles efficiently generated products (**3f**, **3i**) in 84%–99% yields. It was worth mentioning that when varying the alkyl substituents at the *C3*-position of oxindole skeleton, the reactions were also compatible with the catalytic system and led to products **3k**-**3m** in decent 58%–78% yields. Additionally, 3-cyanomethyl and heterocyclic substituents proved viable as well, providing the related products (**3n**-**3r**) in 65%–99% yields. Oxindoles with different substituents on the benzene ring also participated in the reactions smoothly. For example, substrates with methyl, methoxy, fluoro, or ester groups on the oxindole framework could also deliver geranyl products (**3s**-**3x**) in good yields (82%–95%).

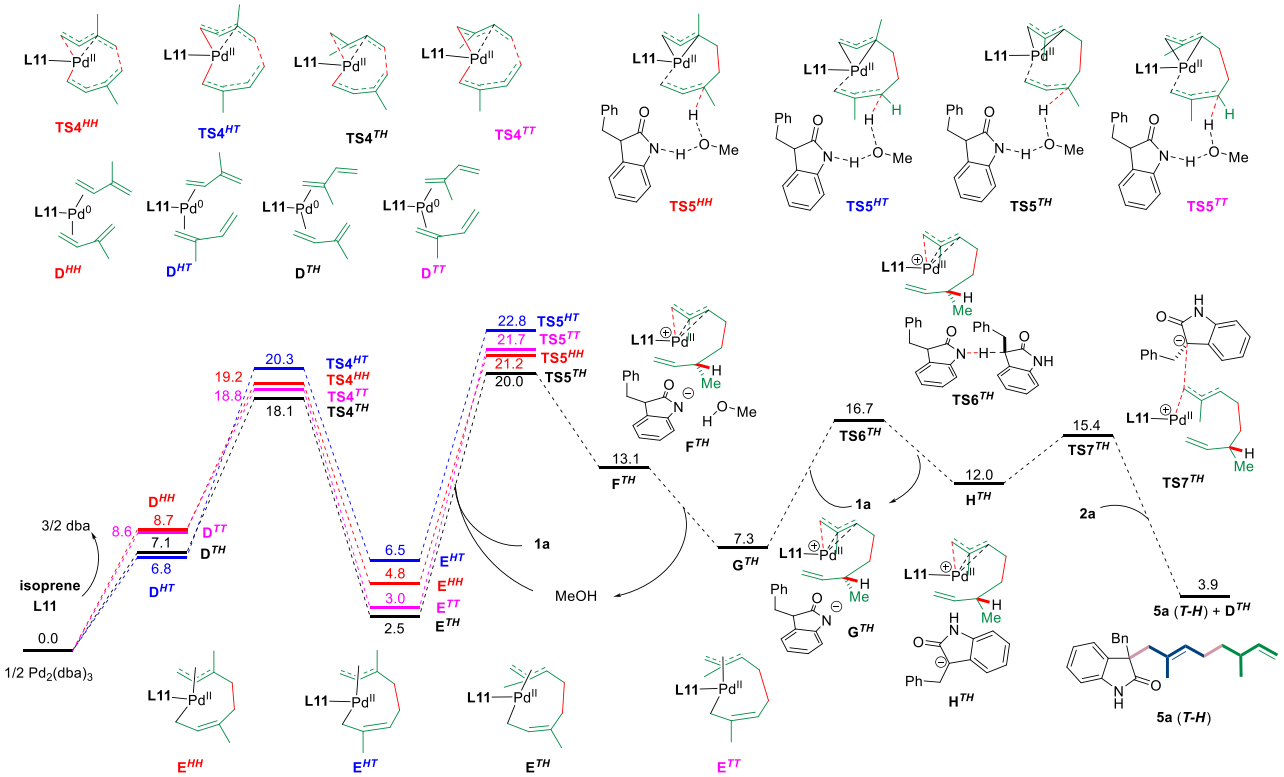

FIGURE 7 | DFT calculations for the tail-to-head telomerization with **L11** as ligand in MeOH. B3LYP-D3BJ/SDD (Pd), 6-311+G(d,p)/SMD(MeOH)//B3LYP/lanl2dz (Pd), and 6-31G(d,p) 60°C (333.15 K).

Although the selective telomerization of isoprene with diethylamine has been extensively studied [32, 34, 39], the tolerance of substrate scope has still remained as an intractable task [32]. Delightfully, our established protocol can also be applied to a broad type of amine nucleophiles. As shown in Figure 3b, both cyclic and acyclic alkyl amines readily underwent the reactions, affording the corresponding products in 96%–99% yields (**9a**-**c**) with excellent regioselectivity. Indoline was a feasible substrate as well, delivering the tail-to-tail (*T-T*) geranylated product **9d** in good 86% yield and 96:4 rr. Notably, the C3-disubstituted oxindole could also undergo telomerization with isoprene smoothly at the *N1*-position, although the regioselectivity slightly diminished (**9e** and **10e**).

The substrate scope for Pd-catalyzed tail-to-head (*T-H*) telomerization was then evaluated in MeOH at 60°C using either **L11** or **L22** as the ligand (Figure 4a). In general, ligand **L22** exhibited superior regioselective control compared to **L11**. However, the latter showed enhanced telomerization reactivity in some cases. Both telomerization protocols displayed a broad scope for *C3*-benzyl-substituted oxindoles: electron-donating or electron-withdrawing groups (e.g., Me, ^{t}Bu, Ph, F) on the benzyl moiety were well tolerated, leading to *T-H* products (**5a–5h**) in good yields (up to 98%) and high regioselectivities (up to 93:7 *rr*). Other *C3*-alkyl-substituted oxindoles were also suitable substrates for the *T-H* geranylation reactions (**5i–5j**). However, a decrease in regioselectivity was observed for the cyanomethyl-substituted oxindole (**5k**), presumably due to its strong coordinating ability. To our delight, *N*-protected oxindole exhibited better performance in both yield and regioselectivity in the reactions with **L22** as the ligand (**5a** vs. **5l**, **5k** vs. **5o**). And heterocyclic substituents, such as pyridinyl and furyl at the *C3* position were also compatible, affording the corresponding products **5m** and **5n** in good yields and acceptable regioselectivities. Modifications of the oxindole framework with electron-donating (Me, OMe) or electron-withdrawing (F, CF_3, CO_2Me) groups at different positions were all feasible, providing *T-H* telomers (**5p–5t**) in high yields (up to 99%), with regioselectivity remaining at a decent level throughout these transformations. Notably, the C3-substituent of oxindole is crucial to ensure the reactivity and selectivity. Subjecting indolin-2-ones to the standard conditions, the telomerization reactions were completely impeded or accompanied by complicated side products (Figure S5).

The Pd_2dba_3/**L22** catalysis also effectively promoted the geranylation of various amines in *T-H* selectivity, even when the Pd loading was decreased to 0.5 mol% (Figure 4b). Secondary amines, whether cyclic or acyclic, all afforded products **11a–d** in excellent yields with up to 95:5 *rr*. The *T-H* telomerization of benzylamines was also effective, although the regioselectivity was slightly eroded (**11e**-**g**). Remarkably, the geranylation of amino alcohols under the current conditions showed exclusive chemoselectivity for the amino group over the hydroxy group, giving products **11 h** and **11i** in 90% and 75% yields, respectively. Sterically hindered amines with acetal or adamantyl groups were tolerated as well (**11j–k**). Apart from aliphatic amines, anilines were also viable substrates. Among them, anilines bearing electron-rich groups (*p*-Me, *p*-^{t}Bu, 3,5-Me) smoothly delivered *T-H* isomers **11l–n**. Interestingly, primary alkyl amines with small substituents led to the formation of bis-geranylated products **11o–11q** in moderate yields of 34%–44%.

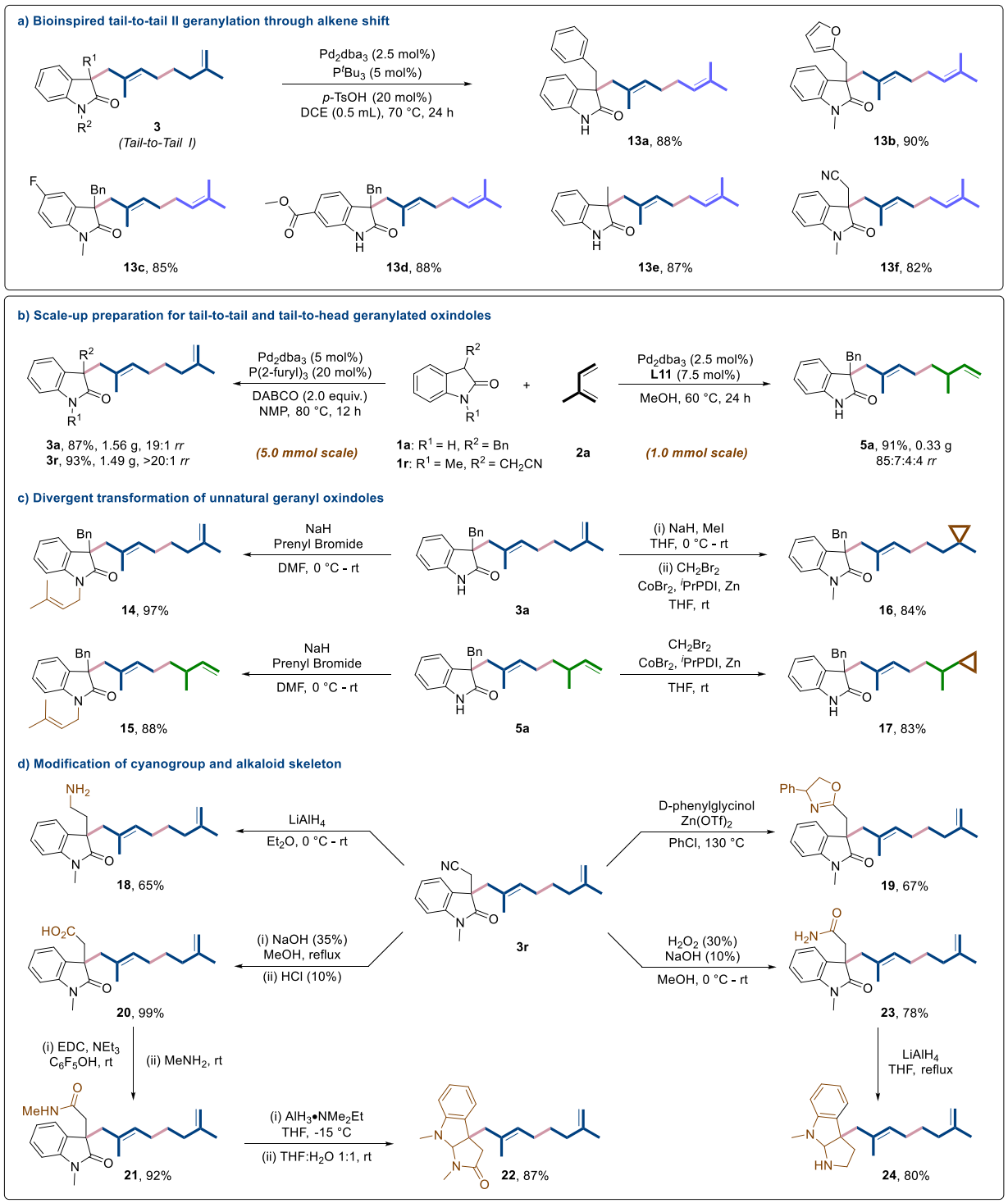

FIGURE 8 | Scale-up preparation and divergent transformation.

To gain mechanistic insights into the tail-to-tail telomerization of isoprene with oxindole, we prepared several Pd catalytic precursors with different phosphine ligand, such as $[(acac)Pd(PPh_3)_2]BF_4$ **[Pd-PPh$_3$]**, $[(acac)Pd(TFP)_2]BF_4$ **[Pd-TFP]** and $[(acac)Pd(dppp)]BF_4$ **[Pd-dppp]** (see Supporting Information for details) [55, 56]. Then the reactivity of these [Pd-L] precursors was evaluated under standard condition in the coupling of isoprene with oxindole (Table S23, entries 1–3). Only telomerized products were produced under [**Pd-PPh$_3$**] and [**Pd-TFP**] catalysis and the tail-to-tail product **3a** was generated in 88% yield (> 20:1 *rr*) with the aid of [**Pd-TFP**], while [**Pd-dppp**] catalysis mainly led to 1:1-adducts (**7a**, **8a**). Reaction of [**Pd-TFP**] with isoprene in the presence of reductant zinc powder and acetone successfully delivered a mixture of bis(allyl)-Pd intermediate **B** and **E** with a low-field signal at −15.7 and −15.2 ppm observed via in situ ^{31}P NMR analysis (Figures 5a and S23). Moreover, subjecting such intermediates to couple with oxindole **2a** through an in situ procedure could produce

telomeric products in 59%, 11%, and 5% yield respectively (*T-T*, *T-H*, and *H-T*), indicating that the bis(allyl)-Pd complex is probably the active intermediate for this telomerization (Figure 5a). To clarify the ligation state of palladium metal with hemilabile phosphine ligands (**L9**), the reactions of phosphine ligands (Ph-JohnPhos **L1** and **L9**), $[Pd(allyl)Cl]_2$ and $AgBF_4$ were conducted to synthesize **[Pd-L]** complexes (Figure 5b) [57]. While a single signal at 22.6 ppm was found for **[Pd-Ph-JohnPhos]** complex via ^{31}P NMR analysis (Figure S30), two signals at 21.3 and 20.7 ppm (1.6:1) were found for complexes arise from **L9** (Figure S32), possibly attributes to the existence of Pd-carbonyl coordination (Figure 5b, **[Pd-9]** and **[Pd-L9]′)**. To verify this, infrared radiation absorption spectra were conducted with **L9** and **Pd-L9** complex respectively. It showed that the intensity of IR absorption peak for unsymmetric stretching vibration ($\nu_{C\text{-}O\text{-}C}$) for **Pd-L9** complex was enhanced and underwent redshift compared with spectra for **L9** (Figure S33). These results indicate the ester group in phosphine ligand **L9** probably might act as hemilabile coordinated site with Pd^{II} center.

Kinetic experiments showed an approximately linear correlation between product yield and reaction time for both **3a** and **5a** under standard conditions, indicative of a steady catalytic process (Figure 5c). Deuterium-labeling experiments were then conducted to get more mechanistic insights (Figure 5d). In the *tail-to-tail* telomerization, the addition of CH_3OD led to product **3a-*d*** in 48% yield with 61% deuterium at *C6* site of geranyl chain. In comparison, subjecting oxindole ***N*-Me-1a-*d*** with 90% D at *C3*-position to the standard reaction condition also delivered product **3o-*d*** with 82% deuteration rate at *C6* site of geranyl chai. For the tail-to-head telomerization, the use of CH_3OD as solvent gave the product **5a-*d*** (64% yield, 71:8:17:4 *rr*) with 94% deuterium at *C6* site of geranyl chain. When ***N*-Me-1a-*d*** (90% D at *C3*-position) was added in CH_3OD, product **5l-*d*** was obtained in 71% yield with 100% deuterium at *C6* site. These results indicate that the protonolysis process takes place at *C6* site of the bis(allyl)-Pd intermediate. When the *tail-to-tail* telomerization proceeds in an aprotic solvent (NMP), the proton source involved in the protonolysis process should be directly derived from the C(3)-H of oxindole (see Figure 6). Conversely, the alcohol may participate in the protonolysis when MeOH added, as illustrated by the DFT calculation (see Figure 7). In addition, our supplementary experiments confirmed that H–D exchange between the C(3)-H of oxindole and MeOD was feasible under the standard conditions, with deuteration incorporations of 65% and 78%, respectively (Figure S24c). Therefore, it remains difficult to determine whether the proton source originates from the alcohol or the oxindole when reactions were conducted in protic solvent. Moreover, oxindole (***N*-Me-1a**) and deuterated oxindole (***N*-Me-1a-*d***) were reacted in parallel under condition A and condition B, respectively (Figure 5e). The observation of a substantial kinetic isotope effect (KIE = 2.1) in the *tail-to-tail* telomerization pathway suggests the protonation of the bis(allyl)-Pd intermediate might be the rate-determining step. A measurable *KIE* (1.6) was also found for the tail-to-head telomerization pathway, implying that protonation step probably contributed to the rate-limiting process as well.

To further elucidate the mechanism and understand the origin of its regioselectivity, density functional theory (DFT) calculations were performed for this Pd-catalyzed telomerization on a model reaction with oxindole **1a** and isoprene **2a**. Based on our mechanistic experiments and related reports [31–38], the reaction may mainly undergo three fundamental steps: oxidative cyclization between two isoprene molecules and Pd(0) precursor, protolysis and nucleophilic substitution. For the *T-T* telomerization reaction (Figures 6 and S34), the Pd(0) initially coordinates with two isoprene molecules assisted by $P(2\text{-furyl})_3$ ligand. Due the nonsymmetric structure, the isoprene unit may coordinate with Pd(0) in the presence of $P(2\text{-furyl})_3$ ligand at either head- or tail-site, leading to three Pd(0)-alkene complexes (Int $\mathbf{A^{HH}}$, $\mathbf{A^{HT/TH}}$, and $\mathbf{A^{TT}}$). Then oxidative cyclization proceeds through transition state **TS1**, delivering four possible palladacycles (Int $\mathbf{B^{HH}}$, $\mathbf{B^{HT}}$, $\mathbf{B^{TH}}$, and $\mathbf{B^{TT}}$). The transition state barrier of this oxidative cyclization step is relatively low ($\Delta G^{\ddagger}$ = 10.6–12.0 kcal/mol, **TS1**). The base additive, DABCO, may act as proton shuttle by assisting the deprotonation of oxindole and then promoting the protolysis of palladacycle **B** to generate allyl-Pd(II) intermediate **C** (Figures S6 and S7). This transition state is calculated to be energetical climax and is speculated a rate-limiting step. In this context, the Boltzmann distribution of the relative energies was calculated based on **TS2** (pages S77). The predicted isomer distribution is 94%, 5%, <1%, and <1% for telomers **3a**, **4a**, **5a**, and **6a**, respectively. This distribution was in excellent agreement with the experimental values (97%, 7%, n. d., and n. d., Table 1, entry 14). Investigations by Jolly and our group all indicated that the formation of (η^1,η^3-$Me_2C_8H_{10}$)Pd complex may be reversible [38, 58]. The lowest energy barrier was found for tail-tail (*T-T*) dimer ($\Delta G^{\ddagger}$ = 20.4 kcal/mol, $\mathbf{TS2^{TT}}$), while the energy barrier for *T-H* dimer was highest ($\Delta G^{\ddagger}$ = 24.1 kcal/mol, $\mathbf{TS2^{TH}}$). Finally, nucleophilic substitution of **Int** $\mathbf{C^{TT}}$ with oxindole anion via **TS3** ($\Delta G^{\ddagger}$ = 12.8 kcal/mol) releases *T-T* telomer **3a** as preferential product and regenerates active Pd(0) catalyst.

For Pd-catalyzed tail-to-head telomerization, the DFT calculations were performed using **L11** as ligand for simplicity (Figures 7 and S35), which indicates that the reaction oxidative cyclization step of Pd(0)-alkene complexes (**Int D**) may also proceed in an equilibrium prior to the next catalytic step ($\Delta G^{\ddagger}$ = 10.2–13.5 kcal/mol, **TS4**). For the protolysis, methanol may work as a proton shuttle under current condition, enabling a proton to migrate from the *N*-atom of the oxindole to the allylic position of the isoprene unit (**Int E**). Among all isomers in this process, the transition state of *T-H* dimer ($\mathbf{TS5^{TH}}$) was found to have the lowest relative energy (20.0 kcal/mol). The NH proton of 3-benzyloxindole is proposed to activate methanol through hydrogen-bonding interactions. Given that *N*-protected oxindoles can also undergo these reactions, we performed additional DFT calculations on distinct protonolysis pathways starting from intermediate $\mathbf{E^{TH}}$ (Figure S36). The results indicate that direct protonolysis by MeOH—without hydrogen-bond activation by the NH moiety of 3-benzyloxindole—is also viable for reactions employing *N*-protected oxindoles ($\mathbf{TS5\text{-}1^{TH}}$, $\Delta G^{\ddagger}$ = 25.0 kcal/mol, Figure S36). In contrast, the ligand-to-ligand hydrogen transfer (LLHT) pathway is less favorable due to its higher energy barrier ($\mathbf{TS5\text{-}2^{TH}}$, $\Delta G^{\ddagger}$ = 28.8 kcal/mol, Figure S36). Besides, the calculations of the Boltzmann distribution based on **TS5** showed that predicted isomer distribution for telomers **3a**, **4a**, **5a**, and **6a** is 6%, 1%, 80%, and 13%, respectively (pages S78). The isomer distribution was also in agreement with the experimental values (4%, 1%, 87%, and 8%, Table S19, entry 4). After protolysis step, the reaction preferentially delivers the *T-H* telomeric allyl-Pd(II) cation and oxindole nitrogen anion (**Int** $\mathbf{F^{TH}}$ and its de-methanolization

Int GTH). Subsequently, the ion migration occurs from nitrogen to benzylic carbon atom through the introduction of second oxindole molecule **1a** (TS6, $\Delta G^{\ddagger}$ = 9.4 kcal/mol), leading to an ionic pair consisting of the allyl-Pd(II) cation and the oxindole carbon anion (**HTH**). In the end, nucleophilic substitution via transition state **TS7TH** ($\Delta G^{\ddagger}$ = 3.4 kcal/mol) gives the tail-to-head coupling product **5a** and recycles the palladium catalysis.

The tail-to-tail products **3** can be further isomerized to internal skipped diene *tail-to-tail II* products **13** via Pd-H catalysis (Figure 8a) [59]. After optimization (Table S24) [60], the product **13a** could be obtained in 88% yield with the aid of bulky ligand P(^{t}Bu)$_3$ and acid *p*-TsOH in dichloroethane. The 2-furyl heterocyclic substituted geranyl oxindole also went smoothly in the isomerization process to provide **13b** in 90% yield. Oxindoles bearing electron-withdrawing groups (F and CO_2Me) were all compatible and gave the corresponding products in good yields (**13c** and **13d**). Additionally, geranylated oxindoles with alkyl substituents at *C3*-position produced internal skipped diene products in 87% and 82% yields as well (**13e** and **13f**).

To further illustrate the practical utility of this telomerization protocol, scale-up experiments were performed (Figure 8b). The tail-to-tail geranyl products **3a** and **3r** could both be obtained in gram scale with good yields and regioselectivity (5.0 mmol scale, 1.56 and 1.49 g, respectively). The tail-to-head geranyl product **5a** was also isolated in 91% total yield in the presence of **L11** (1.0 mmol scale, 0.33 g). The unnatural geranyl oxindoles could be transformed to various products by manipulating the geranyl olefin, cyano motif and oxindole skeleton (Figure 8c,d). For example, geranyl 3-Bn oxindoles **3a** and **5a** could be further modified by nucleophilic substitution with prenyl bromide at *N1* site to give prenylated products **14** and **15** in 97% and 88% yields. The terminal olefin unit at the geranyl group of telomeric products **3a** and **5a** could undergo the cobalt-catalyzed Simmons-Smith reaction to deliver cyclopropanation products **16** and **17** in 84% and 83% yields [61]. In the presence of $LiAlH_4$, the reduction of geranyl acetonitrile **3r** was carried out to access a primary amine **18** in 65% yield [62]. Besides, **3r** could be condensed with amino alcohol to form oxazoline **19** in 67% yield [63, 64]. The hexahydropyrrolo[2,3-*b*]indole are very important skeleton in many natural products and synthetic pharmaceuticals [65–67]. To our delight, geranyl hexahydropyrrolo[2,3-*b*]indole **22** could be prepared smoothly through stepwise hydrolysis, amidation and reductive annulation reactions from product **3r**. Alternatively, the hydrolysis of product **3r** in the presence of H_2O_2, followed by one-pot reduction and ring-closure by $LiAlH_4$ also delivered product **24** as hexahydropyrrolo[2,3-*b*]indole skeleton in good efficiency.

3 | Conclusion

In conclusion, a regiodivergent Pd-catalyzed telomerization of isoprene with oxindoles has been achieved through synergistic manipulation of ligands, solvents and additives. With DABCO as additive, excellent tail-to-tail (*T-T*) selectivity can be achieved with TFP as ligand in aprotic polar solvent. In contrast, the selectivity is switched to tail-to-head (*T-H*) coupling products in the presence of hemilabile phosphine ligands when protic MeOH was employed as solvent. Through mechanistic experiments and DFT calculations, the oxidative cyclization is found to be reversible and rate-determining step is speculated to the protolysis process. The synthetic utility is also demonstrated by Pd-catalyzed alkene isomerization and a series of derivatizations of the geranyl olefin, cyano group, and oxindole skeletons. This strategy expands monoterpenoid diversity beyond biosynthetic *H-T* limitations, advancing synthetic access to unnatural terpenoids for pharmaceutical exploration.

Author Contributions

Ying-Ying Liu: conceptualization, investigation, methodology, validation, software, formal analysis, data curation, writing – original draft, and writing – review and editing. **Shao-Han Sun:** conceptualization, investigation, writing – original draft, methodology, validation, writing – review and editing, software, formal analysis, and data curation. **Xue-Ting Li:** validation, data curation, writing – original draft, and writing – review and editing. **Zhi-Hui Wang:** data curation, validation, writing – review and editing, and writing – original draft. **Ding-Wei Ji:** conceptualization, investigation, methodology, validation, software, formal analysis, data curation, supervision, writing – original draft, writing – review and editing, funding acquisition, visualization, project administration, and resources. **Xiang-Ping Hu:** conceptualization, investigation, funding acquisition, writing – original draft, methodology, validation, visualization, writing – review and editing, software, formal analysis, project administration, data curation, supervision, and resources. **Qing-An Chen:** conceptualization, investigation, funding acquisition, writing – original draft, methodology, validation, visualization, writing – review and editing, software, formal analysis, project administration, data curation, supervision, and resources.

Acknowledgments

Financial support from the Natural Science Foundation of Liaoning Province (2024JH3/50100006) and the National Natural Science Foundation of China (22371275, 22201281) is acknowledged.

Conflicts of Interest

The authors declare no conflicts of interest.

Data Availability Statement

The data that support the findings of this study are available in the Supporting Information of this article.

References

1. D. Urabe, T. Asaba, and M. Inoue, "Convergent Strategies in Total Syntheses of Complex Terpenoids," *Chemical Reviews* 115 (2015): 9207–9231, https://doi.org/10.1021/cr500716f.

2. C. S. Harmange Magnani, D. Q. Thach, K. T. Haelsig, and T. J. Maimone, "Syntheses of Complex Terpenes From Simple Polyprenyl Precursors," *Accounts of Chemical Research* 53 (2020): 949–961, https://doi.org/10.1021/acs.accounts.0c00055.

3. M. Teng, W. Zi, and D. Ma, "Total Synthesis of the Monoterpenoid Indole Alkaloid (±)-Aspidophylline A," *Angewandte Chemie International Edition* 53 (2014): 1814–1817, https://doi.org/10.1002/anie.201310928.

4. J. D. Mason and S. M. Weinreb, "Total Syntheses of the Monoterpenoid Indole Alkaloids (±)-Alstoscholarisine B and C," *Angewandte Chemie International Edition* 56 (2017): 16674–16676, https://doi.org/10.1002/anie.201710943.

5. X. Zhang, B. N. Kakde, R. Guo, S. Yadav, Y. Gu, and A. Li, "Total Syntheses of Echitamine, Akuammiline, Rhazicine, and Pseudoakuam-

migine," *Angewandte Chemie International Edition* 58 (2019): 6053–6058, https://doi.org/10.1002/anie.201901086.

6. M. Idrees, F. L. Hakkim, G. A. Naikoo, and I. U. Hassan, "Recent Advances in Extraction, Characterization, and Potential Use of Citral" in *Natural Bio-active Compounds* (Springer, 2019): 225–236, https://doi.org/10.1007/978-981-13-7438-8_9.

7. H. Yaakob, F. Husin, and S. Baba, et al., "Bioencapsulation for the functional foods and nutraceuticals," in *Smart Nanomaterials for Bioencapsulation* (Elsevier, 2022): 125–155, https://doi.org/10.1016/B978-0-323-91229-7.00008-8.

8. S. Reis, A. Mantello, J. Macedo, et al., "Typical Monoterpenes as Insecticides and Repellents against Stored Grain Pests," *Molecules* 21 (2016): 258, https://doi.org/10.3390/molecules21030258.

9. M. E. Davies, D. Tsyplenkov, and V. J. J. Martin, "Engineering Yeast for De Novo Synthesis of the Insect Repellent Nepetalactone," *ACS Synthetic Biological* 10 (2021): 2896–2903, https://doi.org/10.1021/acssynbio.1c00420.

10. L. Ruzicka, "The Isoprene Rule and the Biogenesis of Terpenic Compounds," *Experientia* 9 (1953): 357–367, https://doi.org/10.1007/BF02167631.

11. K. Chen and P. S. Baran, "Total Synthesis of Eudesmane Terpenes by Site-Selective C–H Oxidations," *Nature* 459 (2009): 824–828, https://doi.org/10.1038/nature08043.

12. E. Oldfield and F. Y. Lin, "Terpene Biosynthesis: Modularity Rules," *Angewandte Chemie International Edition* 51 (2011): 1124–1137, https://doi.org/10.1002/anie.201103110.

13. M. Kobayashi and T. Kuzuyama, "Structural and Mechanistic Insight into Terpene Synthases that Catalyze the Irregular Non-Head-to-Tail Coupling of Prenyl Substrates," *ChemBioChem* 20 (2018): 29–33, https://doi.org/10.1002/cbic.201800510.

14. J. N. Whitehead, N. G. H. Leferink, L. O. Johannissen, S. Hay, and N. S. Scrutton, "Decoding Catalysis by Terpene Synthases," *ACS Catalysis* 13 (2023): 12774–12802, https://doi.org/10.1021/acscatal.3c03047.

15. D. W. Christianson, "Structural and Chemical Biology of Terpenoid Cyclases," *Chemical Reviews* 117 (2017): 11570–11648, https://doi.org/10.1021/acs.chemrev.7b00287.

16. H.-F. Tu, X. Zhang, C. Zheng, M. Zhu, and S.-L. You, "Enantioselective Dearomative Prenylation of Indole Derivatives," *Nature Catalysis* 1 (2018): 601–608, https://doi.org/10.1038/s41929-018-0111-8.

17. K. Takahash, G. Hata, and A. Miyake, "Dimerization of Isoprene by Palladium-Diphosphine Complex Catalyst," *Bulletin of the Chemical Society of Japan* 46 (1973): 600–602, https://doi.org/10.1246/bcsj.46.600.

18. A. D. Josey, "Palladium-Catalyzed Linear Dimerization of Conjugated Dienes," *Journal of Organic Chemistry* 39 (1974): 139–145, https://doi.org/10.1021/jo00916a004.

19. J. P. Neilan, R. M. Laine, N. Cortese, and R. F. Heck, "Monoterpene Syntheses via a Palladium Catalyzed Isoprene Dimerization," *Journal of Organic Chemistry* 41 (1976): 3455–3460, https://doi.org/10.1021/jo00883a030.

20. L. I. Zakharkin, S. A. Babich, and I. V. Pisareva, "Telomerization of Isoprene With Water and Acetic Acid Under the Influence of Complex Palladium Catalysts," *Bulletin of the Academy of Sciences of the USSR, Division of chemical science* 25 (1976): 1531–1533, https://doi.org/10.1007/BF00920834.

21. W. Keim, K. R. Kurtz, and M. Roper, "Palladium Catalyzed Telomerization of Isoprene With Secondary Amines and Conversion of the Resulting Terpene Amines to Terpenols," *Journal of Molecular Catalysis* 20 (1983): 129–138, https://doi.org/10.1016/0304-5102(83)83002-8.

22. L. I. Zakharkin, E. A. Petrushkina, and L. S. Podvisotskaya, "Telomerization of Isoprene With Piperidine on Complex Palladium Catalysts," *Bulletin of the Academy of Sciences of the USSR, Division of chemical science* 32 (1983): 805–809, https://doi.org/10.1007/BF00953482.

23. L. I. Zakharkin and E. A. Petrushkina, "Telomerization of Isoprene With N-Methylaniline on Complex Palladium Catalysts," *Bull Acad Sci USSR, Div Chem Sci* 35 (1986): 1219–1222, https://doi.org/10.1007/BF00956601.

24. I. Maluenda, M.-T. Chen, D. Guest, S. M. Roe, M. L. Turner, and O. Navarro, "Room Temperature, Solventless Telomerization of Isoprene with Alcohols Using (N-Heterocyclic Carbene)–Palladium Catalysts," *Catalysis Science & Technology* 5 (2015): 1447–1451, https://doi.org/10.1039/C5CY00058K.

25. W. Zahreddine, Q. Lelong, I. Karamé, et al., "Synthesis of Terpene Derivatives of Ethanolamine Using Telomerization Reaction," *Tetrahedron Letters* 57 (2016): 452–457, https://doi.org/10.1016/j.tetlet.2015.12.075.

26. G. Wilke, B. Bogdanovič, P. Borner, et al., "Cyclooligomerization of Butadiene and Transition Metal π-Complexes," *Angewandte Chemie International Edition* 2 (1963): 105–115, https://doi.org/10.1002/anie.196301051.

27. R. Baker, "π-Allylmetal derivatives in organic synthesis," *Chemical Reviews* 73 (1973): 427–530, https://doi.org/10.1021/cr60285a004.

28. Y. Yamamoto and N. Asao, "Selective Reactions Using Allylic Metals," *Chemical Reviews* 93 (1993): 2207–2293, https://doi.org/10.1021/cr00022a010.

29. T. Sandmeier, F. W. Goetzke, S. Krautwald, and E. M. Carreira, "Iridium-Catalyzed Enantioselective Allylic Substitution With Aqueous Solutions of Nucleophiles," *Journal of the American Chemical Society* 141 (2019): 12212–12218, https://doi.org/10.1021/jacs.9b05830.

30. J. Yang, P. Wang, H. Neumann, R. Jackstell, and M. Beller, "Industrially Applied and Relevant Transformations of 1,3-Butadiene Using Homogeneous Catalysts," *Industrial Chemistry & Materials* 1 (2023): 155–174, https://doi.org/10.1039/D3IM00009E.

31. R. Jackstell, A. Grotevendt, D. Michalik, L. El Firdoussi, and M. Beller, "Telomerization and Dimerization of Isoprene by In Situ Generated Palladium–Carbene Catalysts," *Journal of Organometallic Chemistry* 692 (2007): 4737–4744, https://doi.org/10.1016/j.jorganchem.2007.06.039.

32. J. Colavida, J. A. Lleberia, A. Salom-Català, et al., "Regioselectivity Control in Pd-Catalyzed Telomerization of Isoprene Enabled by Solvent and Ligand Selection," *ACS Catalysis* 10 (2020): 11458–11465, https://doi.org/10.1021/acscatal.0c02911.

33. F. Leca and R. Reau, "2-Pyridyl-2-Phospholenes: New P,N Ligands for the Palladium-Catalyzed Isoprene Telomerization," *Journal of Catalysis* 238 (2006): 425–429, https://doi.org/10.1016/j.jcat.2006.01.010.

34. S. M. Maddock and M. G. Finn, "Palladium-Catalyzed Head-to-Head Telomerization of Isoprene With Amines," *Organometallics* 19 (2000): 2684–2689, https://doi.org/10.1021/om000286g.

35. C. Y. Zhao, Y. Y. Liu, X. X. Zhang, et al., "Bioinspired and Ligand-Regulated Unnatural Prenylation and Geranylation of Oxindoles With Isoprene Under Pd Catalysis," *Angewandte Chemie International Edition* 61 (2022): e202207202, https://doi.org/10.1002/anie.202207202.

36. W. S. Zhang, D. W. Ji, Y. Yang, et al., "Nucleophilic Aromatization of Monoterpenes From Isoprene Under Nickel/Iodine Cascade Catalysis," *Nature Communications* 14 (2023): 7087, https://doi.org/10.1038/s41467-023-42847-6.

37. G. Zhang, C. Y. Zhao, X. T. Min, et al., "Nickel-Catalysed Asymmetric Heteroarylative Cyclotelomerization of Isoprene," *Nature Catalysis* 5 (2022): 708–715, https://doi.org/10.1038/s41929-022-00825-z.

38. X.-Y. Wang, B.-Z. Chen, S.-Y. Xu, et al., "Nickel-Catalyzed Arylative Telomerization of Isoprene," *Nature Communications* 16 (2025): 9952, https://doi.org/10.1038/s41467-025-64893-y.

39. J. Colavida, R. G. Penido, A. Collado, et al., "Palladium-Catalyzed Telomerization of Isoprene with Amines: Ligands and Solvents Working Together to Improve the Selectivity," *ChemCatChem* 17 (2025): e00786, https://doi.org/10.1002/cctc.202500786.

40. A. D. Marchese, E. M. Larin, B. Mirabi, and M. Lautens, "Metal-Catalyzed Approaches Toward the Oxindole Core," *Accounts of Chemical Research* 53 (2020): 1605–1619, https://doi.org/10.1021/acs.accounts.0c00297.

41. Y.-Y. Liu, Y. Li, X.-T. Li, et al., "Unified Construction of Prenylated and Reverse-Prenylated Oxindoles From Isoprene Launched by Ni Catalysis," *Chinese Journal of Catalysis* 70 (2025): 444–454, https://doi.org/10.1016/S1872-2067(24)60218-4.

42. Y. C. Hu, X. T. Min, D. W. Ji, and Q. A. Chen, "Catalytic Prenylation and Reverse Prenylation of Aromatics," *Trends Chem* 4 (2022): 658–675, https://doi.org/10.1016/j.trechm.2022.04.004.

43. Y. C. Hu, D. W. Ji, C. Y. Zhao, H. Zheng, and Q. A. Chen, "Catalytic Prenylation and Reverse Prenylation of Indoles With Isoprene: Regioselectivity Manipulation Through Choice of Metal Hydride," *Angewandte Chemie International Edition* 58 (2019): 5438–5442, https://doi.org/10.1002/anie.201901025.

44. C. S. Kuai, D. W. Ji, C. Y. Zhao, H. Liu, Y. C. Hu, and Q. A. Chen, "Ligand-Regulated Regiodivergent Hydrosilylation of Isoprene Under Iron Catalysis," *Angewandte Chemie International Edition* 59 (2020): 19115–19120, https://doi.org/10.1002/anie.202007930.

45. W. S. Jiang, D. W. Ji, W. S. Zhang, et al., "Orthogonal Regulation of Nucleophilic and Electrophilic Sites in Pd-Catalyzed Regiodivergent Couplings between Indazoles and Isoprene," *Angewandte Chemie International Edition* 60 (2021): 8321–8328, https://doi.org/10.1002/anie.202100137.

46. G. Zhang, W. S. Zhang, X. Y. Wang, et al., "Ni-Catalyzed Unnatural Prenylation and Cyclic Monoterpenation of Heteroarenes With Isoprene," *Chinese Journal of Catalysis* 49 (2023): 123–131, https://doi.org/10.1016/S1872-2067(23)64437-7.

47. D. Wang, B. Dong, Y. Wang, et al., "Rhodium-Catalysed Direct Hydroarylation of Alkenes and Alkynes With Phosphines Through Phosphorous-Assisted C–H Activation," *Nature Communications* 10 (2019): 3539, https://doi.org/10.1038/s41467-019-11420-5.

48. Z. Zhang, T. Roisnel, P. H. Dixneuf, and J. F. Soulé, "Rh I-Catalyzed P III-Directed C–H Bond Alkylation: Design of Multifunctional Phosphines for Carboxylation of Aryl Bromides With Carbon Dioxide," *Angewandte Chemie International Edition* 58 (2019): 14110–14114, https://doi.org/10.1002/anie.201906913.

49. L. Lin, X. Zhang, X. Xu, Y. Zhao, and Z. Shi, "$Ru_3(CO)_{12}$-Catalyzed Modular Assembly of Hemilabile Ligands by C−H Activation of Phosphines with Isocyanates," *Angewandte Chemie International Edition* 62 (2023): e202214584, https://doi.org/10.1002/anie.202214584.

50. Z. Li and Z. Shi, "Late-Stage Diversification of Phosphines by C–H Activation: A Robust Strategy for Ligand Design and Preparation," *Accounts of Chemical Research* 57 (2024): 1057–1072, https://doi.org/10.1021/acs.accounts.4c00020.

51. K. Tian, X. Q. Dong, and C. J. Wang, "Cu/Ru Relay Catalysis Enables Functionalization of Allenic Alcohols With Stereodivergence and Skeleton Diversity," *Journal of the American Chemical Society* 147 (2025): 33288–33303, https://doi.org/10.1021/jacs.5c12469.

52. M. Q. Tang, Z. J. Yang, A. J. Han, and Z. T. He, "Diastereoselective and Enantioselective Hydrophosphinylations of Conjugated Enynes, Allenes and Dienes via Synergistic Pd/Co Catalysis," *Angewandte Chemie International Edition* 64 (2025): e202413428, https://doi.org/10.1002/anie.202413428.

53. P. Luo, J. Li, Y. H. Deng, et al., "Switchable Chemo-, Regio- and Pseudo-Stereodivergence in Palladium-Catalyzed Cycloaddition of Allenes," *Angewandte Chemie International Edition* 63 (2024): e202412179, https://doi.org/10.1002/anie.202412179.

54. Deposition Numbers 2425139 (for **L16**), 2425232 (for **L20**), and 2425141 (for **L24**) Contain the Supplementary Crystallographic Data for this Paper. These data are provided free of charge by the Cambridge Crystallographic Data Centre and Fachinformationszentrum Karlsruhe Access Structures Service.

55. V. S. Tkach, D. S. Suslov, G. Myagmarsuren, et al., "An Effective Route for the Synthesis of Cationic Palladium Complexes of General Formula $[(Acac)PdL^1L^2]+A-$," *Journal of Organometallic Chemistry* 693 (2008): 2069–2073, https://doi.org/10.1016/j.jorganchem.2007.12.019.

56. D. S. Suslov, M. V. Bykov, M. V. Belova, P. A. Abramov, and V. S. Tkach, "Palladium(II)–Acetylacetonate Complexes Containing Phosphine and Diphosphine Ligands and Their Catalytic Activities in Telomerization of 1,3-Dienes With Diethylamine," *Journal of Organometallic Chemistry* 752 (2014): 37–43, https://doi.org/10.1016/j.jorganchem.2013.11.017.

57. S. Seo, J. Jung, and H. Kim, "Palladium-Catalyzed Hydrosilylation of Unactivated Alkenes and Conjugated Dienes With Tertiary Silanes Controlled by Hemilabile Hybrid P,O Ligand," *Angewandte Chemie International Edition* 62 (2023): e202303853, https://doi.org/10.1002/anie.202303853.

58. R. Benn, P. W. Jolly, R. Mynott, et al., "Intermediates in the Palladium-Catalyzed Reactions of 1,3-Dienes. 2. Preparation and Structure of (.eta.1,.eta.3-Octadienediyl)Palladium Complexes," *Organometallics* 4 (1985): 1945–1953, https://doi.org/10.1021/om00130a005.

59. D. Gauthier, A. T. Lindhardt, E. P. K. Olsen, J. Overgaard, and T. Skrydstrup, "In Situ Generated Bulky Palladium Hydride Complexes as Catalysts for the Efficient Isomerization of Olefins. Selective Transformation of Terminal Alkenes to 2-Alkenes," *Journal of the American Chemical Society* 132 (2010): 7998–8009, https://doi.org/10.1021/ja9108424.

60. S. Sanz-Navarro, M. Mon, A. Doménech-Carbó, et al., "Parts–Per–Million of Ruthenium Catalyze the Selective Chain–Walking Reaction of Terminal Alkenes," *Nature Communications* 13 (2022): 2831, https://doi.org/10.1038/s41467-022-30320-9.

61. J. Werth and C. Uyeda, "Regioselective Simmons–Smith-Type Cyclopropanations of Polyalkenes Enabled by Transition Metal Catalysis," *Chemical Science* 9 (2018): 1604–1609, https://doi.org/10.1039/C7SC04861K.

62. M. H. Sun, L. S. Wei, and C. K. Li, "Regio- and Enantioselective Allylic Cyanomethylation by Synergistic Rhodium and Silane Catalysis," *Journal of the American Chemical Society* 145 (2023): 3897–3902, https://doi.org/10.1021/jacs.3c00244.

63. C. Bolm, K. Weickhardt, M. Zehnder, and T. Ranff, "Synthesis of Optically Active Bis(2-Oxazolines): Crystal Structure of a 1,2-Bis(2-Oxazolinyl)Benzene $ZnCl_2$ Complex," *Chemische Berichte* 124 (1991): 1173–1180, https://doi.org/10.1002/cber.19911240532.

64. E. Pires, J. I. García, A. Cornejo, et al., "An Efficient and General One-Pot Method for the Synthesis of Chiral Bis(Oxazoline) and Pyridine Bis(Oxazoline) Ligands," *Synlett* (2005): 2321–2324, https://doi.org/10.1055/s-2005-872672.

65. Y. Hou, J. Y. Huo, R. X. Li, et al., "Catalytic Asymmetric Reverse Prenylation of Indol-2-One Enabled a Synthesis of (−)-Debromoflustramine A," *Organic Letters* 25 (2023): 6949–6953, https://doi.org/10.1021/acs.orglett.3c02296.

66. B. M. Trost, S. Malhotra, and W. H. Chan, "Exercising Regiocontrol in Palladium-Catalyzed Asymmetric Prenylations and Geranylation: Unifying Strategy Toward Flustramines A and B," *Journal of the American Chemical Society* 133 (2011): 7328–7331, https://doi.org/10.1021/ja2020873.

67. E. M. Marlett and W. S. Park, "Dimethylethylamine Alane and N-Methylpyrrolidine Alane. A Convenient Synthesis of Alane, a Useful Selective Reducing Agent in Organic Synthesis," *Journal of Organic Chemistry* 55 (1990): 2968–2969, https://doi.org/10.1021/jo00296a078.

Supporting Information

Additional supporting information can be found online in the Supporting Information section.

Supporting File 1: anie72888-sup-0001-SuppMat.pdf.

Supporting File 2: anie72888-sup-0002-cif.zip.